

FL Games: A federated learning framework for distribution shifts

Sharut Gupta^{1,2,3}, Kartik Ahuja³, Mohammad Havaei¹, Niladri Chatterjee², and
Yoshua Bengio³

¹Imagia Cybernetics, Montréal, Canada

²Indian Institute of Technology Delhi, New Delhi, India

³Mila - Quebec AI Institute, Université de Montréal, Quebec, Canada ,

{sharut.gupta,mt617,niladri.chatterjee}@maths.iitd.ac.in

{sharut.gupta,mohammad}@imagia.com

{sharut.gupta,kartik.ahuja,yoshua.bengio}@mila.quebec

May 24, 2022

Abstract

Federated learning aims to train predictive models for data that is distributed across clients, under the orchestration of a server. However, participating clients typically each hold data from a different distribution, whereby predictive models with strong in-distribution generalization can fail catastrophically on unseen domains. In this work, we argue that in order to generalize better across non-i.i.d. clients, it is imperative to only learn correlations that are stable and invariant across domains. We propose FL GAMES, a game-theoretic framework for federated learning for learning causal features that are invariant across clients. While training to achieve the Nash equilibrium, the traditional best response strategy suffers from high-frequency oscillations. We demonstrate that FL GAMES effectively resolves this challenge and exhibits smooth performance curves. Further, FL GAMES scales well in the number of clients, requires significantly fewer communication rounds, and is agnostic to device heterogeneity. Through empirical evaluation, we demonstrate that FL GAMES achieves high out-of-distribution performance on various benchmarks.

Keywords: Federated Learning, Out-of-Distribution Generalization, Causal Inference, Invariant Learning

1 Introduction

With the rapid advance in technology and growing prevalence of smart devices, Federated Learning (FL) has emerged as an attractive distributed learning paradigm for machine learning models over networks of computers [Kairouz et al. \(2019\)](#); [Li et al. \(2020\)](#); [Bonawitz et al. \(2019\)](#). In FL, multiple sites with local data, often known as *clients*, collaborate to jointly train a shared model under the orchestration of a central hub called the *server*.

While FL serves as an attractive alternative to centralized training because the client data need not be sent to the server, there are several challenges associated with its optimization: 1) *statistical heterogeneity* across clients; 2) *massively distributed with limited communication* i.e, a large number of client devices with only a small subset of active clients at any given time [McMahan et al. \(2017\)](#); [Li et al. \(2020\)](#). One of the most popular algorithms in this setup, Federated Averaging (FEDAVG) [McMahan et al. \(2017\)](#), allows multiple updates at

each site prior to communicating updates with the server. While this technique delivers huge communication gains in i.i.d. (independent and identically distributed) setting, its performance on non-i.i.d. clients is an active area of research. As shown by Karimireddy et al. (2020), client heterogeneity has direct implications on the convergence of FEDAVG since it introduces a *drift* in the updates of each client with respect to the server model. While recent works Li et al. (2019); Karimireddy et al. (2020); Yu et al. (2019); Wang et al. (2020); Li et al. (2020); Lin et al. (2020); Li & Wang (2019); Zhu et al. (2021) have tried to address client heterogeneity through constrained gradient optimization and knowledge distillation, most did not tackle the underlying distribution shift. These methods mostly adapt variance reduction techniques such as Stochastic Variance Reduction Gradients (SVRG) Johnson & Zhang (2013) to FL. The bias among clients is reduced by constraining the updates of each client with respect to the aggregated gradients of all other clients. These methods can at best generalize to interpolated domains and fail to extrapolate well, i.e., generalize to new extrapolated domains¹. Further, since these works do not extract causal features, they might have poor generalization to the distribution of a test client unseen during training.

According to Pearl (2018) and Schölkopf (2019), learning robust predictors that are free from spurious correlations requires an altogether different approach that goes beyond standard statistical learning. In particular, they emphasize that in order to build robust systems that generalize well outside of their training environment, learning algorithms should be equipped with causal reasoning tools. Over the past year, there has been a surge in interest in bringing the machinery of causality into machine learning Arjovsky et al. (2019); Ahuja et al. (2020); Schölkopf (2019); Ahuja et al. (2021b); Parascandolo et al. (2020); Robey et al. (2021); Krueger et al. (2021); Rahimian & Mehrotra (2019). All these approaches have focused on learning causal dependencies, which are stable across training domains and further estimate a truly invariant and causal predictor. Inspired by the invariance principle Peters et al. (2016), Invariant Risk Minimization (IRM) Arjovsky et al. (2019) introduces an alternative training objective that aims at learning representations that are invariant across domains. Invariant Risk Minimization Games (IRM GAMES) reformulates the training objective proposed by IRM as an ensemble game and utilizes game-theoretic tools to learn invariant predictors (i.e., that remain accurate across domains). Formally, they establish the equivalence between the set of predictors that solve the Nash equilibrium of the ensemble game and the set of invariant predictors across the training domains.

Since FL typically consists of a large number of clients, it is natural for data at each client to represent different annotation tools, measuring circumstances, experimental environments and external interventions. Predictive models trained on such datasets could simply rely on spurious correlations to improve their in-distribution i.i.d. performance. Inspired by the recent progress in causal machine learning, we take a causal perspective to tackle the challenge of client heterogeneity under distribution shifts in federated learning. Specifically, we propose an algorithm for learning causal representations which are stable across clients and further enhance the generalizability of the trained model across out-of-distribution (OOD) datasets. Our algorithm draws motivation from IRM GAMES. We argue that, in contrast to IRM, IRM GAMES lends itself naturally to FL, where each client serves as a player that competes to optimize its local objective. Furthermore, the server orchestrates the optimization towards the global objective. However, despite its efficacy across multiple benchmarks, IRM GAMES has several key limitations that render it inapplicable in the FL setting.

- **Sequential dependency.** The underlying game theoretic algorithm in IRM GAMES

¹Similar to Krueger et al. (2021), we define interpolated domains as the domains which fall within the convex hull of training domains and extrapolated domains as those that fall outside of that convex hull.

is inherently sequential. This causes the time complexity of the algorithm to scale linearly with the number of environments.

- **Oscillations.** IRM GAMES show that large oscillations in the performance metrics emerge as the training progresses. The high frequency of these oscillations makes it difficult to define a valid stopping criterion.
- **Convergence speed.** The convergence speed of IRM GAMES has direct implications on the number of communication rounds in a FL setting.

In this study, we introduce Federated Learning Games (FL GAMES) and address each of the above challenges. We summarize our main contributions below.

- We propose a new framework called FL GAMES for learning causal representations that are invariant across clients in a federated learning setup.
- Inspired from the game theory literature, we equip our algorithm to allow parallel updates across clients, further resulting in superior scalability.
- Using ensembles over client’s historical actions, we demonstrate that FL GAMES appreciably smoothen the observed oscillations.
- By increasing the local computation at each client, we show that FL GAMES significantly reduces the number of communication rounds.
- Empirically, we show that the invariant predictors found by our approach lead to better or comparable performance than [Ahuja et al. \(2020\)](#) on several benchmarks.

2 Related works

Federated learning (FL). A major challenge in federated learning is data heterogeneity across clients where the local optima at each client may be far from that of the global optima in the parameter space. This causes a *drift* in the local updates of each client with respect to the server aggregated parameters and further results in slow and unstable convergence [Karimireddy et al. \(2020\)](#). Recent works have shown FEDAVG to be vulnerable in such heterogeneous settings [Zhao et al. \(2018\)](#). A subset of these works that explicitly constrains gradients for bias removal are called extra gradient methods. Among these methods, FEDPROX [Li et al. \(2020\)](#) imposes a quadratic penalty over the distance between server and client parameters which impedes model plasticity. Others use a form of variance reduction techniques such as SVRG [Johnson & Zhang \(2013\)](#) to regularize the client updates with respect to the gradients of other clients [Acar et al. \(2021\)](#); [Li et al. \(2019\)](#); [Karimireddy et al. \(2020\)](#); [Liang et al. \(2019\)](#); [Zhang et al. \(2020\)](#); [Konečný et al. \(2016\)](#). [Karimireddy et al. \(2020\)](#) communicates to the server an additional set of variables known as control variates which contain the estimate of the update direction for both the server and the clients. Using these control variates, the drift at each client is estimated and used to correct the local updates. On the other hand, [Acar et al. \(2021\)](#) estimates the drift for each client on the server and corrects the server updates. By doing so, they avoid using control variates and consume less communication bandwidth. The general strategy for variance reduction methods is to estimate client drift using gradients of other clients, and then constrain the learning objective to reduce the drift. The extra gradient methods are not explicitly optimized to discover causal features, and thus may fail when introduced with out-of-distribution examples outside the aggregated distribution of the set of clients.

To date, only two scientific works Francis et al. (2021); Tenison et al. (2021) have incorporated the learning of invariant predictors in order to achieve strong generalization in FL. The former adapts masked gradients Parascandolo et al. (2020) and the latter builds on IRM to exploit invariance and improve leakage protection in FL. While IRM lacks theoretical convergence guarantees, failure modes of Parascandolo et al. (2020) like formation of dead zones and high sensitivity to small perturbations Shahtalebi et al. (2021), translate to FL, rendering it unreliable.

Out-of-distribution (OOD) generalization. Generalization under distributional shift is one of the major challenges faced by machine learning systems, limiting their application in the real world. Recent research Arjovsky et al. (2019); Ahuja et al. (2020); Schölkopf (2019); Ahuja et al. (2021b); Parascandolo et al. (2020); Robey et al. (2021); Krueger et al. (2021); Rahimian & Mehrotra (2019); Xie et al. (2020); Yao et al. (2022); Ahuja et al. (2021a) has tried to address this challenge by proposing alternative objectives for training mechanisms that are invariant across training environments. IRM Arjovsky et al. (2019) proposes finding a representation $\phi(X)$ that has good prediction abilities and also elicits an invariant predictor across environments. Works like Krueger et al. (2021); Xie et al. (2020) propose penalty over a function of variance of training risks. Ahuja et al. (2020) reformulates IRM as finding the Nash equilibrium of an ensemble game played among several environments. Mahajan et al. (2021) argues learning invariant representations for inputs derived from the same object. Recently, Robey et al. (2021) proposed Model-Based Domain Generalization, which enforces invariance to the underlying transformations of data. Another line of work Rosenfeld et al. (2020); Kamath et al. (2021); Ahuja et al. (2021a) has theoretically analyzed the failure modes of IRM.

3 Background

3.1 Federated Averaging (FEDAVG)

Federated learning methods involve a cloud server coordinating among multiple client devices to jointly train a global model without sharing data across clients. We assume that there is a cloud server that can both send and receive message from m client devices. Denote \mathcal{S} to be the set of client devices. Let N_k denote the number of data samples at client device k , and $\mathcal{D}_k = \{(x_i^k, y_i^k)\}_{i=1}^{N_k}$ as it's labelled dataset. Mathematically, the objective of a FL is to minimize the approximation of global loss

$$\min_w F(w) \text{ where } F(w) := \sum_{k=1}^m \frac{1}{m} \sum_{i=1}^{N_k} \frac{1}{N_k} \ell(x_i^k, y_i^k, w), \quad (1)$$

where ℓ is the loss function and w is the model parameter. One of the most popular methods in FL is Federated Averaging (FEDAVG), where each client performs E local-updates before communicating its weights with the server. FEDAVG becomes equivalent to FEDSGD for $E = 1$ wherein weights are communicated after every local update. For each client device k , FEDAVG initializes it's corresponding device model w_k^0 . Consequently, in round t , each device undergoes a local update on its dataset according to the following

$$w_k^{t+1} \leftarrow w_k^t - \eta^k \nabla \ell(\mathcal{B}_i^k, w_k^t), \quad \forall \mathcal{B}_i^k \subseteq \mathcal{D}_k$$

where \mathcal{B}_i^k is a sampled mini-batch from \mathcal{D}_k at the i th step. All clients' models $\{w_k^{t+1}\}_{k \in \mathcal{S}}$ are then broadcasted to the cloud server which performs a weight average to update the global model w^{t+1} as

$$w^{t+1} \leftarrow \frac{1}{|\mathcal{S}|} \sum_{k \in \mathcal{S}} \frac{N_k}{N} w_k^t,$$

where N_k is the number of samples at client device k and N is the total number of samples from all clients ($N = \sum_{k=1}^m N_k$). This aggregated global model is shared with all clients and the above process is repeated till convergence.

3.2 Invariant Risk Minimization and Invariant Risk Minimization Games

Consider a setup comprising datasets $\mathcal{D}_k = \{(x_i^k, y_i^k)\}_{i=1}^{N_k}$ from multiple training environments, $k \in \mathcal{E}_{tr}$ with N_k being the number of samples at environment k . The aim of Invariant Risk Minimization (IRM) [Arjovsky et al. \(2019\)](#) is to jointly train across all these environments and learn a robust set of parameters θ that generalize well to unseen (test) environments $\mathcal{E}_{all} \supset \mathcal{E}_{tr}$. The risk of a predictor f at each environment can be mathematically represented as $R^k(w \circ \phi) = E_{(x,y) \sim D_k} f_\theta((w \circ \phi); x, y)$ where $f_\theta = w \circ \phi$ is the composition of a feature extraction function $\phi: \mathcal{X} \rightarrow \mathcal{Z} \subseteq \mathbb{R}^d$ and a predictor network, $w: \mathcal{Z} \rightarrow \mathbb{R}^k$ where k is the number of classes.

Empirical Risk Minimization (ERM) aims to minimize the average of the losses across all environments. Mathematically, the ERM objective can be formulated as $R^{\text{ERM}}(\theta) = E_{(x,y) \sim \cup_{e \in \mathcal{E}} D_e} f_e(\theta; x, y)$. As shown in [Arjovsky et al. \(2019\)](#), ERM fails to generalize to novel domains, which have significant distribution shift as compared to the training environments.

Invariant Risk Minimization (IRM) instead aims to capture invariant representations ϕ such that the optimal predictor w given ϕ is the same across all training environments. Mathematically, they formulate the objective as a bi-level optimization problem

$$\min_{\phi \in \mathcal{H}_\phi, w \in \mathcal{H}_w} \sum_{k \in \mathcal{E}_{tr}} R^k(w \circ \phi) \text{ s.t. } w \in \arg \min_{w \in \mathcal{H}_w} R^k(w \circ \phi), \forall k \in \mathcal{E}_{tr} \quad (2)$$

where \mathcal{H}_ϕ , \mathcal{H}_w are the hypothesis sets for feature extractors and predictors, respectively. Since each constraint calls an inner optimization routine, IRM approximates this challenging optimization problem by fixing the predictor w to a scalar.

Invariant Risk Minimization Games (IRM GAMES) is an algorithm based on an alternate game theoretic reformulation of the optimization objective in equation 2. It endows each environment with its own predictor $w^k \in \mathcal{H}_w$ and aims to train an ensemble model $w^{av}(z) = \frac{1}{|\mathcal{E}_{tr}|} \sum_{k=1}^{|\mathcal{E}_{tr}|} w^k(z)$ for each $z \in \mathcal{Z}$ s.t. w^{av} satisfies the following optimization problem

$$\begin{aligned} & \min_{w^{av}, \phi \in \mathcal{H}_\phi} \sum_k R^k(w^{av} \circ \phi) \\ & \text{s.t. } w^k \in \arg \min_{w'_k \in \mathcal{H}_w} R^k \left(\frac{1}{|\mathcal{E}_{tr}|} (w'_k + \sum_{q \in \mathcal{E}_{tr}, q \neq k} w^q) \circ \phi \right), \forall k \in \mathcal{E}_{tr} \end{aligned} \quad (3)$$

The constraint in equation 3 is equivalent to the Nash equilibrium of a game with each environment k as a player with action w^k , playing to maximize its utility $R^k(w^{av}, \phi)$. While there are different algorithms in the game theoretic literature to compute the Nash equilibrium, the resultant non-zero sum continuous game is solved using the best response dynamics (BRD) with clockwise updates and is referred to as V-IRM GAMES. In this training paradigm, players take turns according to a fixed cyclic order and only one player is allowed to change its action at any given time (for more details, refer to the supplement). Fixing ϕ to an identity map in V-IRM GAMES is also showed to be very effective and is called F-IRM GAMES.

4 Federated Learning Games

4.1 Invariant risk minimization games as a natural fit for federated learning

OOD generalization is often studied using the notion of environments. Arjovsky et al. (2019) formalize an environment as a data-generating distribution representing a particular location, time, context, circumstances and so forth. Distinct environments are assumed to share some overlapping causal features. Spurious variables denote unstable features which vary across environments. A client in FL can be considered as a data-generating environment. For instance, consider a FL system with clients being hospitals, each collecting mammographic data for breast cancer detection. However, heterogeneity in acquisition systems, patient population, disease prevalence, etc can result in spurious correlations which are unique to a client. While these correlations differ across clients, features predictive of microcalcifications remain invariant.

That said, IRM GAMES, initially developed to tackle OOD generalization, can be naturally adapted to FL. In particular, each client now serves as a player, competing to optimize its local objective, i.e. $\min_{w'_k \in \mathcal{H}_w} R^k \left(\frac{1}{|\mathcal{E}_{tr}|} (w'_k + \sum_{q \neq k} w^q) \circ \phi \right), \forall k \in \mathcal{E}_{tr}$ (Equation 3). The server acts as a mechanism designer which ensures the prediction efficacy of the models by optimizing the upper level objective of equation 3 i.e. $\min_{w^{av}, \phi \in \mathcal{H}_\phi} \sum_k R^k(w^{av} \circ \phi)$. IRM GAMES permit local computation at each client and yet is guaranteed to exhibit good out-of-distribution generalization behavior (See Ahuja et al. (2021b)), such guarantees do not exist for other works that explore invariance in federated learning (Tenison et al., 2021; Francis et al., 2021). Further, IRM GAMES doesn't require additional regularization parameters for which the coefficient needs to be tuned.

4.2 Limitations of IRM GAMES

IRM GAMES has proved to be effective in the identification of non-spurious causal feature-target interactions across a variety of benchmarks. Although widely used in the machine learning community, there are several challenges which limit its utility in the FL domain. We shall elaborate on each of these limitations and propose solutions to make it feasible for its practical deployment in FL setup.

Sequential dependency As discussed in Section 3.2, IRM GAMES poses the IRM objective as that of finding the Nash equilibrium of an ensemble game across training environments and adopts the classic best response dynamics (BRD) algorithm to compute it. This approach is based on playing clockwise sequences wherein players take turns in a fixed cyclic order, with only one player being allowed to change its action at any given time t (details in the supplement). In order to choose its optimal action for the first time steps, the last scheduled player N has to wait for all the remaining players from $1, 2, \dots, N-1$ to play their strategies. This linear scaling of time complexity with the number of players poses a major challenge for adapting IRM GAMES to FL setup, which requires fast convergence and should exploit computational parallelism across the clients.

By definition, in BRD with clockwise playing sequences, the best responses of any player determine the best responses of the remaining players. Thus, in a distributed learning paradigm, the best responses of each client (player) need to be transmitted to all the other clients. This is infeasible from a practical standpoint as clients are usually based on slow or expensive connections and message transmissions can frequently get delayed or result in information loss. Hence, it is imperative to develop scalable and efficient FL algorithms which are able to learn causal features and at the same time require minimal information about the actions of other clients in the system. As shown on lines 20 and 26 (green) of

Algorithm 1, we modify the classic BRD algorithm by allowing simultaneous updates at any given time t . We refer to this variant of F-IRM GAMES and V-IRM GAMES as *parallelized* F-IRM GAMES and, V-IRM GAMES respectively.

Oscillations. As demonstrated by Ahuja et al. (2020), when a neural network is trained using the IRM GAMES objective (equation 3), the training accuracy initially stabilizes at a high value and eventually starts to oscillate. The setup over which these observations are made involves two training environments with varying degrees of spurious correlation. The environments are constructed so that the degree of correlation of color with the target label is very high. The explanation for these oscillations attributes the problem to the significant difference among the data of the training environments. In particular, after a few steps of training, the individual model of the environment with higher spurious correlation (say \mathcal{E}_1) is positively correlated with the color while the other is negatively correlated. When it is the turn of the former environment to play its optimal strategy, it tries to exploit the spurious correlation in its data and increase the weights of the neurons which are indicative of color. On the contrary, the latter tries to decrease the weights of features associated with color since the errors that backpropagate are computed over the data for which exploiting spurious correlation does not work (say \mathcal{E}_2). This continuous swing and sway among individual models may explain the observed oscillations.

Despite the promising results, with a model’s performance metrics oscillating at each step, defining a reasonable stopping criterion becomes challenging. As shown in the game theoretic literature Herings & Predtetchinski (2017); Barron et al. (2010); Fudenberg et al. (1998); Ge et al. (2018), BRD can often oscillate. Computing the Nash equilibrium for general games is non-trivial and is only possible for a certain class of games (e.g., concave games) (Zhou et al., 2017). Thus, rather than alleviating oscillations completely, we propose solutions to reduce them significantly to better identify valid stopping points. We propose a two-way ensemble approach wherein apart from maintaining an ensemble across clients (w^{av}), each client k responds to the ensemble of historical models (memory) of its opponents. Intuitively, a moving ensemble over the historical models acts as a smoothing filter, which helps to reduce drastic variations like those discussed above.

Based on the above motivation, we reformulate the optimization objective of IRM GAMES (Equation 3) to adapt the two-way ensemble learning mechanism (refer to line 4(red) in Algorithm 1). Formally, we maintain queues (a form of buffer) at each client that store its historically played actions. In each iteration, a client best responds to a uniform distribution over the past strategies of its opponents. Mathematically, the new objective can be stated as

$$\begin{aligned} & \min_{w^{av}, \phi \in \mathcal{H}_\phi} \sum_k R^k(w^{av} \circ \phi) \\ \text{s.t. } & w^k \in \arg \min_{w'_k \in \mathcal{H}_w} R^k \left(\frac{1}{|\mathcal{E}_{tr}|} (w'_k + \sum_{\substack{q \in \mathcal{E}_{tr} \\ q \neq k}} w^q + \sum_{\substack{p \in \mathcal{E}_{tr} \\ p \neq k}} \frac{1}{|\mathcal{B}_p|} \sum_{j=1}^{|\mathcal{B}_p|} w_j^p) \circ \phi \right), \forall k \in \mathcal{E}_{tr} \end{aligned} \quad (4)$$

where \mathcal{B}_q denotes the buffer at client q and w_j^q denotes the j th historical model of client q . We use the same buffer size for all clients. Moreover, as the buffer reaches its capacity, it is renewed in a first-in first-out (FIFO) manner. This variant is called F-FL GAMES (SMOOTH) or V-FL GAMES (SMOOTH), based on the constraint on ϕ .

Convergence speed. The convergence speed of IRM GAMES has direct implications on the number of communication rounds in the FL setup. As discussed in Section 3.2, Ahuja et al. (2020) propose two variant of IRM GAMES: F-IRM GAMES and, V-IRM GAMES with the former being an approximation of the latter ($\phi = I$). While both approaches

Algorithm 1 *Parallelized FL GAMES (SMOOTH+FAST)*

```
1: Notations:  $\mathcal{S}$  is the set of  $N$  clients;  $\mathcal{B}_k$  and  $\mathcal{P}_k$  denote the buffer and information
   set containing copies of  $\mathcal{B}_i, \forall i \neq k \in \mathcal{S}$  at client,  $k$  respectively.
2: PredictorUpdate(k):
3:   /* Two-way ensemble (across time and clients) game to update predictor at each client  $k$  */
4:    $w_k \leftarrow \text{SGD} \left[ \ell_k \left\{ \frac{1}{n} (w'_k + \sum_{q \in \mathcal{E}_{tr}, q \neq k} w^q + \sum_{p \in \mathcal{E}_{tr}, p \neq k} \frac{1}{|\mathcal{B}_p|} \sum_{j=1}^{|\mathcal{B}_p|} w_j^p) \circ \phi \right\} \right]$ 
5:   Insert  $w_k$  to  $\mathcal{B}_k$ , discard the oldest model in  $\mathcal{B}_k$  if full
6:   return  $w_k$ 
7: RepresentationUpdate(k):
8:   /* Gradient Descent (GD) over entire local dataset at client  $k$  */
9:   for every batch  $b \in \mathcal{B}$  do
10:    Calculate  $\nabla \ell_k(w_{\text{cur}}^{\text{av}} \circ \phi_{\text{cur}}; b)$  and accumulate in  $\nabla \phi_k$ 
11:  return  $\nabla \phi_k$ 
12: Server executes:
13:  Initialize  $w_k, \forall k \in \mathcal{S}$  and  $\phi$ 
14:  while round  $\leq$  max-round do
15:    /* Update representation  $\phi$  at even round parity */
16:    if round is even then
17:      if Fixed-Phi then
18:         $\phi_{\text{cur}} = I$ 
19:      if Variable-Phi then
20:        for each client  $k \in \mathcal{S}$  in parallel do
21:           $\nabla \phi_k = \text{RepresentationUpdate}(k)$ 
22:        /* Update representation  $\phi$  using weighted sum of gradients across clients */
23:         $\phi_{\text{next}} = \phi_{\text{cur}} - \eta \left( \sum_{k \in \mathcal{S}} \frac{N_k}{\sum_{j \in \mathcal{S}} N_j} \nabla \phi_k \right)$ 
24:         $\phi_{\text{cur}} = \phi_{\text{next}}$ 
25:      else
26:        for each client  $k \in \mathcal{S}$  in parallel do
27:           $w_k \leftarrow \text{PredictorUpdate}(k)$ 
28:        /* Client  $k$  updates its information set  $\mathcal{P}_k$  by updating copies of predictors of other clients */
29:        Communicate  $\forall k, \mathcal{P}_k \leftarrow \{w_i, \forall i \neq k \in \mathcal{S}\}$ 
30:      round  $\leftarrow$  round + 1
31:       $w_{\text{cur}}^{\text{av}} = \frac{1}{N} \sum_{k \in \mathcal{S}} w_{\text{cur}}^k$ 
```

exhibit superior performance on a variety of benchmarks, the latter has shown its success in a variety of large scale tasks like language modeling (Peyrard et al., 2021). In spite of its theoretical support, V-IRM GAMES suffers from slower convergence due to an additional round for optimization of ϕ . This renders it inefficient for deployment in the FL setup. To improve the efficiency of the algorithm, we propose replacing the stochastic gradient descent (SGD) over ϕ by a gradient descent (GD) (line 9 (yellow) of Algorithm 1). This allows ϕ to be updated according to gradients accumulated across the entire dataset, as opposed to gradient step over a mini-batch. Intuitively, now at each gradient step, the resultant ϕ takes large steps in the direction of its global optimum, which in our experiments resulted in fast and stable training. This variant of IRM GAMES is referred to V-FL GAMES (FAST).

5 Experiments and Results

5.1 Datasets

Ahuja et al. (2020) tested IRM GAMES over a variety of benchmarks that were synthetically constructed to incorporate color as a spurious feature. These included the colored digits MNIST dataset, i.e. COLORED MNIST and COLORED FASHION MNIST, and we work with the same datasets for our experiments. Additionally, we created another benchmark, SPURIOUS CIFAR10 with a data-generating process resembling that of COLORED MNIST. In this dataset, instead of coloring the images to establish spurious correlation, we add small black patches at various locations in the image. These locations are spuriously correlated with the label. Details on each of the datasets can be found in the supplement. For all the experiments, we report the mean performance of various baselines over 5 runs. The performance of an oracle on each of these datasets is 75% for training and test sets.

Terminologies: In the following analysis, the terms ‘Sequential’ and ‘Parallel’ denote BRD with clockwise playing sequences and simultaneous updates respectively (Lines 20 and 26 of Algorithm 1). Within this categorization, F-IRM GAMES and V-IRM GAMES refer to the federated adaptations of fixed and variable versions of IRM GAMES respectively. The approach used to smoothen out the oscillations (Line 4 of Algorithm 1) is denoted by F-FL GAMES (SMOOTH) or V-FL GAMES (SMOOTH) depending on the constraint on ϕ . The fast variant with high convergence speed is denoted V-FL GAMES (SMOOTH+FAST) (Line 9 of Algorithm 1).

COLORED MNIST (Table 1) From the table, we can observe that both FEDSGD and FEDAVG are unable to generalize to the test set. Intuitively, both the approaches latch onto the spurious features to make predictions. The sequential F-IRM GAMES and V-IRM GAMES achieve 66.56 ± 1.58 and 63.78 ± 1.58 percent testing accuracy, respectively. Amongst our approaches (F-FL GAMES (SMOOTH), V-FL GAMES (SMOOTH+FAST), F-IRM GAMES (Parallel), V-IRM GAMES (Parallel)), V-IRM GAMES (Parallel) achieves the highest testing accuracy i.e. 68.34 ± 5.24 percent. The benefits of this approach are twofold; 1) learning a representation of truly causal features and hence good OOD generalizability, 2) scalability to large numbers of clients (detailed discussion in Section 5.2.1). Further, since all our proposed approaches have high testing performance, none of them relies on the spurious correlations, unlike ERM-based approaches such as FEDSGD and FEDAVG.

COLORED FASHION MNIST (Table 2) Similar to the results on COLORED MNIST, all the proposed algorithms achieve high testing accuracy. Among the baselines, parallelized F-FL GAMES (SMOOTH) achieves the highest test accuracy of 71.26 ± 4.19 percent. Apart from providing the flexibility of efficiently scaling with the number of clients, this approach also reduces the oscillations significantly (detailed discussed in Section 5.2.2).

SPURIOUS CIFAR10 (Table 3) Both ERM-based approaches, FEDSGD and FEDAVG achieve poor testing accuracy. However, F-IRM GAMES (Parallel) achieves the highest testing accuracy of 52.07 ± 1.60 percent.

In all the above experiments, our main algorithm i.e. *parallelized* V-FL GAMES (SMOOTH+FAST) is able to achieve high testing accuracy which is comparable to the maximum performance. Hence, the benefits provided by this approach in terms of 1) robust predictions; 2) scalability; 3) fewer oscillations and 4) fast convergence are not at the cost of performance. While the former is demonstrated by Tables 1, 2 and 3, the latter three are detailed in the following section.

Table 1: COLORED MNIST: Comparison of methods in terms of training and testing accuracy (mean \pm std deviation).

TYPE	ALGORITHM	TRAIN ACCURACY	TEST ACCURACY
Sequential	FEDSGD	84.88 ± 0.16	10.45 ± 0.60
	FEDAVG	84.45 ± 2.69	12.52 ± 4.34
	F-IRM GAMES	55.76 ± 2.03	66.56 ± 1.58
	V-IRM GAMES	56.40 ± 0.03	63.78 ± 1.58
	F-FL GAMES (SMOOTH)	62.83 ± 5.06	66.83 ± 1.83
	V-FL GAMES (SMOOTH+FAST)	61.03 ± 3.11	65.81 ± 3.28
	F-IRM GAMES	58.03 ± 6.22	67.14 ± 2.95
	V-IRM GAMES	52.89 ± 8.03	68.34 ± 5.24
Parallel	F-FL GAMES (SMOOTH)	61.07 ± 1.71	67.21 ± 2.98
	V-FL GAMES (SMOOTH+FAST)	63.11 ± 3.02	65.73 ± 1.53

Table 2: COLORED FASHION MNIST: Comparison of methods in terms of training and testing accuracy (mean \pm std deviation).

TYPE	ALGORITHM	TRAIN ACCURACY	TEST ACCURACY
Sequential	FEDSGD	83.49 ± 1.22	20.13 ± 8.06
	FEDAVG	86.225 ± 0.63	13.33 ± 2.07
	F-IRM GAMES	75.13 ± 1.38	68.40 ± 1.83
	V-IRM GAMES	69.90 ± 4.56	69.90 ± 1.31
	F-FL GAMES (SMOOTH)	75.18 ± 0.37	71.81 ± 1.60
	V-FL GAMES (SMOOTH+FAST)	75.10 ± 0.48	69.85 ± 1.22
	F-IRM GAMES	71.71 ± 8.23	69.73 ± 2.12
	V-IRM GAMES	66.33 ± 9.39	69.85 ± 3.42
Parallel	F-FL GAMES (SMOOTH)	72.81 ± 4.51	71.36 ± 4.19
	V-FL GAMES (SMOOTH+FAST)	71.89 ± 5.58	69.41 ± 5.49

Table 3: SPURIOUS CIFAR10: Comparison of methods in terms of training and testing accuracy (mean \pm std deviation).

TYPE	ALGORITHM	TRAIN ACCURACY	TEST ACCURACY
Sequential	FEDSGD	84.79 ± 0.17	12.57 ± 0.55
	FEDAVG	85.41 ± 1.45	13.11 ± 1.82
	F-IRM GAMES	50.36 ± 2.78	47.36 ± 4.33
	V-IRM GAMES	61.72 ± 7.39	46.07 ± 6.01
	F-FL GAMES (SMOOTH)	64.02 ± 2.08	45.54 ± 1.04
	V-FL GAMES (SMOOTH+FAST)	50.37 ± 4.97	50.94 ± 3.28
	F-IRM GAMES	55.06 ± 2.04	52.07 ± 1.60
	V-IRM GAMES	50.41 ± 3.31	50.43 ± 3.04
Parallel	F-FL GAMES (SMOOTH)	56.98 ± 4.09	49.56 ± 1.36
	V-FL GAMES (SMOOTH+FAST)	45.83 ± 2.44	49.89 ± 5.66

5.2 Ablation Analysis

In this section, we analyze the effect of each of our algorithmic modifications using illustrative figures on the COLORED MNIST dataset. The results on other datasets are similar and are provided in the supplement.

5.2.1 Effect of Simultaneous BRD

We examine the effect of replacing the classic best response dynamics, following Ahuja et al. (2020), with the simultaneous best response dynamics. For these experiments, we

use a more practical environment: (a) more clients are involved, and (b) each client has fewer data. Similar to [Choe et al. \(2020\)](#), we extended the COLORED MNIST dataset by varying the number of clients between 2 and 10. For each setup, we vary the degree of spurious correlation between 70% and 90% for training clients while introducing a mere 10% spurious correlation in the test set. A more detailed discussion of the dataset is provided in the supplement. For F-IRM GAMES, it can be observed from Figure 1(a), as the number of clients in the FL system increases, there is a sharp increase in the number of communication rounds required to reach an equilibrium. However, the same doesn’t hold true for *parallelized* F-IRM GAMES. Further, *parallelized* F-IRM GAMES is able to reach a comparable or higher test accuracy as compared to F-IRM GAMES with significantly lower communication rounds (refer to Table 1(b)).

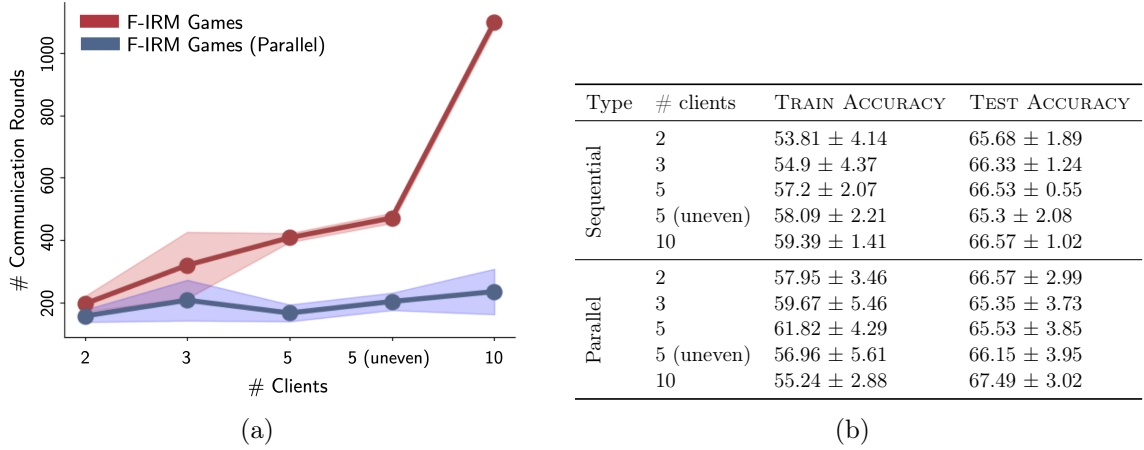


Figure 1: COLORED MNIST: (a) Number of communication rounds required to achieve to achieve Nash equilibrium versus the number of clients in the FL setup; (b) Comparison of F-IRM GAMES and F-IRM GAMES (Parallel) with increasing clients in terms of training and testing accuracy (mean \pm std deviation).

5.2.2 Effect of a memory ensemble

As shown in Figure 2(a), compared to F-IRM GAMES, F-FL GAMES (SMOOTH) reduces the oscillations significantly. In particular, while in the former, performance metrics oscillate at each step, the oscillations in the latter are observed only after an interval of roughly 50 rounds. Further, F-FL GAMES (SMOOTH) seems to envelop the performance curves of IRM GAMES. As a result, apart from reducing the frequency of oscillations, F-FL GAMES (SMOOTH) also achieves higher testing accuracy. This implies that it does not rely on the spurious features to make predictions. Similar performance evolution curves are also observed for *parallelized* F-FL GAMES (SMOOTH) with an added benefit of faster convergence as compared to *parallelized* F-IRM GAMES.

5.2.3 Effect of using Gradient Descent (GD) for ϕ

Communication costs are the principal constraints in FL setup. Edge devices like mobile phones and sensor are bandwidth constrained and require more power for transmission and reception as compared to remote computation. As observed from Figure 2(b), V-FL GAMES (SMOOTH+FAST) is able to achieve significantly higher testing accuracy in fewer communication rounds as compared to V-IRM GAMES.

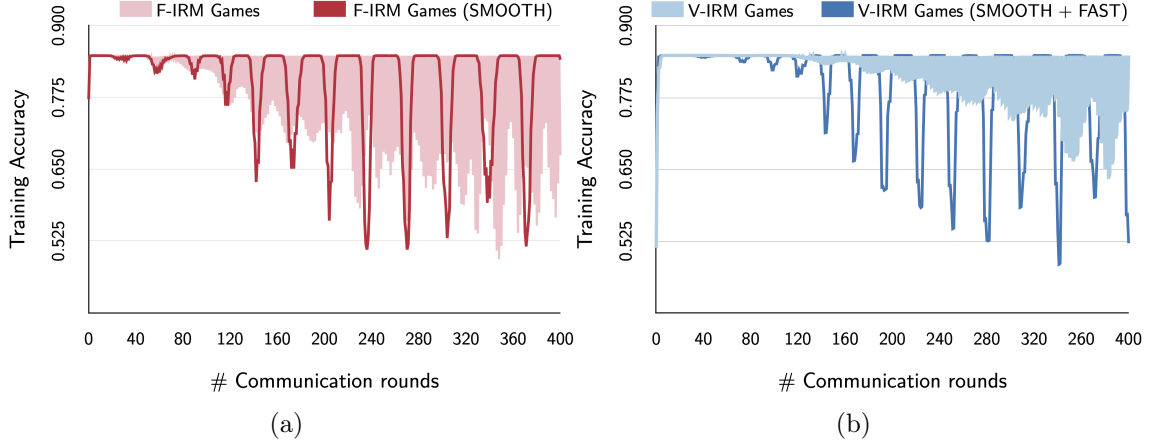


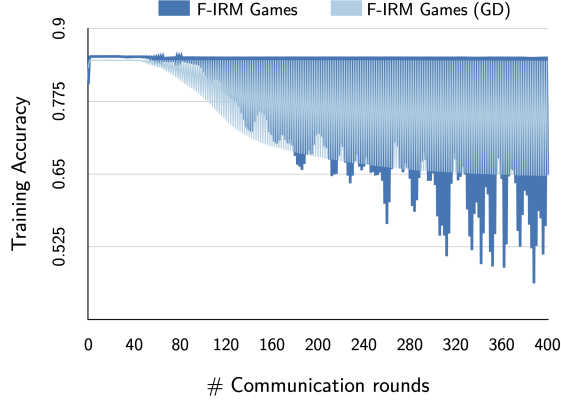
Figure 2: COLORED MNIST: Training accuracy of (a) F-IRM GAMES and F-FL GAMES (SMOOTH) for a buffer size of 5; (b) V-IRM GAMES and V-FL GAMES (SMOOTH+FAST) with buffer size as 5 versus the number of communication rounds.

5.2.4 Effect of exact best response

FEDAVG provides the flexibility to train communication efficient and high-quality models by allowing more local computation at each client. This is particularly detrimental in scenarios with poor network connectivity, wherein communicating at every short time span is infeasible. Inspired by FEDAVG, we study the effect of increasing the amount of local computation at each client. Specifically, in F-IRM GAMES, each client updates its predictor based on a step of stochastic gradient descent over its mini-batch. We modify this setup by allowing each client to run a few steps of stochastic gradient descent locally. When the number of local steps at each client reaches its maximum (training data size/mini-batch size), the scenario becomes equivalent to a gradient descent (GD) over the training data. From Table 3(b), it is evident that as the number of local steps increase i.e. each client **exactly** best responds to its opponents, the testing accuracy at equilibrium starts to decrease. When the local computation reaches 100%, i.e. each client updates its local predictor based on a GD over its data, F-IRM GAMES exhibits reassuring convergence (as shown in Figure 3(a)). IRM GAMES is guaranteed to exhibit convergence and good out-of-distribution generalization behavior (Ahuja et al., 2021b) despite increasing local computations. Although the testing accuracy at convergence is lower compared to the standard setup, this approach opens avenues for practical deployment of the approach in FL.

6 Conclusion

In this work, we develop a novel framework based on the Best Response Dynamics (BRD) training paradigm to learn invariant predictors across clients in Federated learning (FL). Inspired by Ahuja et al. (2020), the proposed method called Federated Learning Games (FL GAMES) learns causal representations which have good out-of-distribution generalization on new training clients or for test clients unseen during training. We investigate the high frequency oscillations observed using BRD and equip our algorithm with a memory of historical actions. This results in smoother evolution of performance metrics, with significantly lower oscillations. FL GAMES exhibits high communication efficiency as it allows parallel computation, scales well in the number of clients and results in faster convergence. Given the impact of FL in medical imaging, we plan to test our framework over medical benchmarks. Future directions include theoretically analyzing the smoothed



(a)

Local steps (in %)	TRAIN ACCURACY	TEST ACCURACY
1.71%	53.04 \pm 1.85	65.05 \pm 1.60
4.27%	55.12 \pm 4.76	61.37 \pm 5.02
6.84%	53.46 \pm 3.66	61.64 \pm 3.67
8.55%	54.13 \pm 5.2	61.07 \pm 5.89
19.66%	54.38 \pm 6.93	59.17 \pm 7.37
29.91%	53.86 \pm 8.14	58.40 \pm 7.19
49.57%	53.59 \pm 8.56	59.22 \pm 6.05
70.09%	54.25 \pm 8.21	58.66 \pm 7.09
80.34%	53.14 \pm 9.86	57.93 \pm 6.23
89.74%	54.61 \pm 7.32	57.76 \pm 6.54
100.00%	54.56 \pm 6.56	57.02 \pm 5.17

(b)

Figure 3: COLORED MNIST: (a) Effect on Training accuracy of doing a gradient descent on each client for updating the predictor versus the standard training paradigm i.e. F-IRM GAMES;(b) Impact of increasing the number of local steps (in % of the maximum number of steps for updating the predictor) on the training and testing accuracy (mean \pm std deviation). When the number of local steps (in %) reaches 100%, it is equivalent to a gradient descent as shown in (a)

best response dynamics, as it might have potential implications for other game-theoretic based machine learning frameworks.

References

- Durmus Alp Emre Acar, Yue Zhao, Ramon Matas Navarro, Matthew Mattina, Paul N Whatmough, and Venkatesh Saligrama. Federated learning based on dynamic regularization. *arXiv preprint arXiv:2111.04263*, 2021.
- Kartik Ahuja, Karthikeyan Shanmugam, Kush Varshney, and Amit Dhurandhar. Invariant risk minimization games. In *International Conference on Machine Learning*, pp. 145–155. PMLR, 2020.
- Kartik Ahuja, Ethan Caballero, Dinghuai Zhang, Jean-Christophe Gagnon-Audet, Yoshua Bengio, Ioannis Mitliagkas, and Irina Rish. Invariance principle meets information bottleneck for out-of-distribution generalization. In A. Beygelzimer, Y. Dauphin, P. Liang, and J. Wortman Vaughan (eds.), *Advances in Neural Information Processing Systems*, 2021a. URL <https://openreview.net/forum?id=jlchsF0LfeF>.
- Kartik Ahuja, Karthikeyan Shanmugam, and Amit Dhurandhar. Linear regression games: Convergence guarantees to approximate out-of-distribution solutions. In *International Conference on Artificial Intelligence and Statistics*, pp. 1270–1278. PMLR, 2021b.
- Martin Arjovsky, Léon Bottou, Ishaan Gulrajani, and David Lopez-Paz. Invariant risk minimization. *arXiv preprint arXiv:1907.02893*, 2019.
- E Barron, Rafal Goebel, and R Jensen. Best response dynamics for continuous games. *Proceedings of the American Mathematical Society*, 138(3):1069–1083, 2010.
- Keith Bonawitz, Hubert Eichner, Wolfgang Grieskamp, Dzmitry Huba, Alex Ingerman, Vladimir Ivanov, Chloe Kiddon, Jakub Konečný, Stefano Mazzocchi, Brendan McMahan, et al. Towards federated learning at scale: System design. *Proceedings of Machine Learning and Systems*, 1:374–388, 2019.
- Yo Joong Choe, Jiyeon Ham, and Kyubyong Park. An empirical study of invariant risk minimization. *arXiv preprint arXiv:2004.05007*, 2020.
- Li Deng. The mnist database of handwritten digit images for machine learning research. *IEEE Signal Processing Magazine*, 29(6):141–142, 2012.
- Sreya Francis, Irene Tenison, and Irina Rish. Towards causal federated learning for enhanced robustness and privacy. *arXiv preprint arXiv:2104.06557*, 2021.
- Drew Fudenberg, Fudenberg Drew, David K Levine, and David K Levine. *The theory of learning in games*, volume 2. MIT press, 1998.
- Hao Ge, Yin Xia, Xu Chen, Randall Berry, and Ying Wu. Fictitious gan: Training gans with historical models. In *Proceedings of the European Conference on Computer Vision (ECCV)*, pp. 119–134, 2018.
- P Jean-Jacques Herings and Arkadi Predtetchinski. Best-response cycles in perfect information games. *Mathematics of Operations Research*, 42(2):427–433, 2017.
- Rie Johnson and Tong Zhang. Accelerating stochastic gradient descent using predictive variance reduction. *Advances in neural information processing systems*, 26:315–323, 2013.
- Peter Kairouz et al. Advances and open problems in federated learning. dec. 10. *arXiv preprint arXiv:1912.04977*, 2019.

- Pritish Kamath, Akilesh Tangella, Danica Sutherland, and Nathan Srebro. Does invariant risk minimization capture invariance? In *International Conference on Artificial Intelligence and Statistics*, pp. 4069–4077. PMLR, 2021.
- Sai Praneeth Karimireddy, Satyen Kale, Mehryar Mohri, Sashank Reddi, Sebastian Stich, and Ananda Theertha Suresh. Scaffold: Stochastic controlled averaging for federated learning. In *International Conference on Machine Learning*, pp. 5132–5143. PMLR, 2020.
- Jakub Konečný, H Brendan McMahan, Daniel Ramage, and Peter Richtárik. Federated optimization: Distributed machine learning for on-device intelligence. *arXiv preprint arXiv:1610.02527*, 2016.
- David Krueger, Ethan Caballero, Joern-Henrik Jacobsen, Amy Zhang, Jonathan Binas, Dinghuai Zhang, Remi Le Priol, and Aaron Courville. Out-of-distribution generalization via risk extrapolation (rex). In *International Conference on Machine Learning*, pp. 5815–5826. PMLR, 2021.
- Daliang Li and Junpu Wang. Fedmd: Heterogenous federated learning via model distillation. *arXiv preprint arXiv:1910.03581*, 2019.
- Tian Li, Anit Kumar Sahu, Manzil Zaheer, Maziar Sanjabi, Ameet Talwalkar, and Virginia Smithy. Feddane: A federated newton-type method. In *2019 53rd Asilomar Conference on Signals, Systems, and Computers*, pp. 1227–1231. IEEE, 2019.
- Tian Li, Anit Kumar Sahu, Manzil Zaheer, Maziar Sanjabi, Ameet Talwalkar, and Virginia Smith. Federated optimization in heterogeneous networks. *Proceedings of Machine Learning and Systems*, 2:429–450, 2020.
- Xianfeng Liang, Shuheng Shen, Jingchang Liu, Zhen Pan, Enhong Chen, and Yifei Cheng. Variance reduced local sgd with lower communication complexity. *arXiv preprint arXiv:1912.12844*, 2019.
- Tao Lin, Lingjing Kong, Sebastian U Stich, and Martin Jaggi. Ensemble distillation for robust model fusion in federated learning. *arXiv preprint arXiv:2006.07242*, 2020.
- Divyat Mahajan, Shruti Tople, and Amit Sharma. Domain generalization using causal matching. In *International Conference on Machine Learning*, pp. 7313–7324. PMLR, 2021.
- Brendan McMahan, Eider Moore, Daniel Ramage, Seth Hampson, and Blaise Agueray Arcas. Communication-efficient learning of deep networks from decentralized data. In *Artificial intelligence and statistics*, pp. 1273–1282. PMLR, 2017.
- Giambattista Parascandolo, Alexander Neitz, Antonio Orvieto, Luigi Gresele, and Bernhard Schölkopf. Learning explanations that are hard to vary. *arXiv preprint arXiv:2009.00329*, 2020.
- Judea Pearl. Theoretical impediments to machine learning with seven sparks from the causal revolution. *arXiv preprint arXiv:1801.04016*, 2018.
- Jonas Peters, Peter Bühlmann, and Nicolai Meinshausen. Causal inference by using invariant prediction: identification and confidence intervals. *Journal of the Royal Statistical Society: Series B (Statistical Methodology)*, 78(5):947–1012, 2016.
- Maxime Peyrard, Sarvjeet Singh Ghotra, Martin Josifoski, Vidhan Agarwal, Barun Patra, Dean Carignan, Emre Kiciman, and Robert West. Invariant language modeling. *arXiv preprint arXiv:2110.08413*, 2021.

- Hamed Rahimian and Sanjay Mehrotra. Distributionally robust optimization: A review. *arXiv preprint arXiv:1908.05659*, 2019.
- Alexander Robey, George Pappas, and Hamed Hassani. Model-based domain generalization. *Advances in Neural Information Processing Systems*, 34, 2021.
- Elan Rosenfeld, Pradeep Ravikumar, and Andrej Risteski. The risks of invariant risk minimization. *arXiv preprint arXiv:2010.05761*, 2020.
- Bernhard Schölkopf. Causality for machine learning. *arXiv preprint arXiv:1911.10500*, 2019.
- Soroosh Shahtalebi, Jean-Christophe Gagnon-Audet, Touraj Laleh, Mojtaba Faramarzi, Kartik Ahuja, and Irina Rish. Sand-mask: An enhanced gradient masking strategy for the discovery of invariances in domain generalization. *arXiv preprint arXiv:2106.02266*, 2021.
- Irene Tenison, Sreya Francis, and Irina Rish. Gradient masked federated optimization. *arXiv preprint arXiv:2104.10322*, 2021.
- Jianyu Wang, Qinghua Liu, Hao Liang, Gauri Joshi, and H Vincent Poor. Tackling the objective inconsistency problem in heterogeneous federated optimization. *arXiv preprint arXiv:2007.07481*, 2020.
- Chuanlong Xie, Haotian Ye, Fei Chen, Yue Liu, Rui Sun, and Zhenguo Li. Risk variance penalization. *arXiv preprint arXiv:2006.07544*, 2020.
- Huaxiu Yao, Yu Wang, Sai Li, Linjun Zhang, Weixin Liang, James Zou, and Chelsea Finn. Improving out-of-distribution robustness via selective augmentation. *arXiv preprint arXiv:2201.00299*, 2022.
- Hao Yu, Rong Jin, and Sen Yang. On the linear speedup analysis of communication efficient momentum sgd for distributed non-convex optimization. In *International Conference on Machine Learning*, pp. 7184–7193. PMLR, 2019.
- Xinwei Zhang, Mingyi Hong, Sairaj Dhople, Wotao Yin, and Yang Liu. Fedpd: A federated learning framework with optimal rates and adaptivity to non-iid data. *arXiv preprint arXiv:2005.11418*, 2020.
- Yue Zhao, Meng Li, Liangzhen Lai, Naveen Suda, Damon Cavin, and Vikas Chandra. Federated learning with non-iid data. *arXiv preprint arXiv:1806.00582*, 2018.
- Zhengyuan Zhou, Panayotis Mertikopoulos, Aris L Moustakas, Nicholas Bambos, and Peter Glynn. Mirror descent learning in continuous games. In *2017 IEEE 56th Annual Conference on Decision and Control (CDC)*, pp. 5776–5783. IEEE, 2017.
- Zhuangdi Zhu, Junyuan Hong, and Jiayu Zhou. Data-free knowledge distillation for heterogeneous federated learning. *arXiv preprint arXiv:2105.10056*, 2021.

7 Supplementary

7.1 Game Theory Concepts

We define some basic game theory notations that will be used later.

Let $\Gamma = (N, \{S_k\}_{k \in N}, \{u_k\}_{k \in N})$ be the tuple representing a normal form game, where N denotes the finite set of players. For each player k , $S_k = \{s_0^k, s_1^k, \dots, s_m^k\}$ denotes the pure strategy space with m strategies and $u_k(s_k, s_{-k})$ denotes the payoff function of player k corresponding to strategy s_k . Here, an environment for player k is s_{-k} , a set containing strategies taken by all players but k and S_{-k} denotes the space of strategies of the opponent players to k . $S = \prod_{i \in N} S_i$ denotes the joint strategy set of all players. A game Γ is said to be finite if S is finite and is continuous if S is uncountably infinite.

While a pure strategy defines a specific action to be followed at any time instance, a mixed strategy of player k , $\sigma_k = \{p_k(s_0^k), p_k(s_1^k), \dots, p_k(s_m^k)\}$ is a probability distribution over a set of pure strategies, where $\sum_{j=1}^m p_k(s_j^k) = 1$. The expected utility of a mixed strategy $u_k(\sigma_k, \sigma_{-k})$ for player k is the expected value of the corresponding pure strategy payoff i.e.

$$\mathbb{E}(u_k(\sigma_k, \sigma_{-k})) = \sum_{s_k \in S_k} \sum_{s_{-k} \in S_{-k}} u_k(s_k, s_{-k}) p_k(s_k) p_{-k}(s_{-k}), \forall \sigma_k \in \tilde{S}_k$$

where \tilde{S}_k corresponds to the mixed strategy space of player k .

Best response (BR). A mixed strategy σ_k^* for player k is said to be a best response to it's opponent strategies σ_{-k} if

$$\mathbb{E}(u_k(\sigma_k^*, \sigma_{-k})) \geq \mathbb{E}(u_k(\sigma_k, \sigma_{-k})), \forall \sigma_k \in \tilde{S}_k.$$

Nash equilibrium. A mixed strategy profile $\sigma^* = \{\sigma_1^*, \sigma_2^*, \dots, \sigma_N^*\}$ is a Nash equilibrium if for all players k , σ_k^* is the best response to the strategies played by it's opponent players i.e σ_{-k}^* .

Best response dynamics (BRD). BRD is an iterative algorithm in which at each time step, a player myopically plays strategies that are best responses to the most recent known strategies played by it's opponents previously. Based on the playing sequence across layers, BRD can be classified into three broad categories: BRD with clockwise sequences, BRD with simultaneous updating and BRD with random sequences. For this study, we focus only on the first two playing schedules. Let the function $\text{seq} : \mathbb{N} \rightarrow \mathcal{P}[N]$ denote a playing sequence which determines the set of players whose turn it is to play at each time period $t \in \mathbb{N}$. Here, $\mathcal{P}[N]$ denotes the power set of $\{1, 2, \dots, N\}$ players and \mathbb{N} be the set of natural numbers $\{1, 2, \dots\}$. By BRD, at each time step t , $\forall i \in \text{seq}(t)$, action taken by player i i.e. a_i^t is the best response to it's current environment i.e a_{-i}^t .

- **BRD with clockwise sequences:** In this playing sequence, players take turns according to a fixed cyclic order and only one player is allowed to change it's action at any given time t . Specifically, the playing sequence is defined by $\text{seq}(t) = 1 + (t - 1) \bmod n$. Since only a single player is allowed to play at any given time t , $a_{-\text{seq}(t)}^t = a_{-\text{seq}(t)}^{t-1}$.
- **BRD with simultaneous updating:** In this playing sequence, $\text{seq}(t)$ chooses a non empty subset of players to participate in round t . However, for each player $i \in \text{seq}(t)$, the optimal action chosen a_i^t depends on the knowledge of the latest strategy of it's opponents.

7.2 Datasets

The MNIST dataset consists of handwritten digits, with a total of 60,000 images in the training set and 10,000 images in the test set [Deng \(2012\)](#). These images are black and

white in colour and form a subset of the larger collection of digits called NIST. Each digit in the dataset is normalized in size to centre fit in the fixed size image of size 28×28 . It is then anti-aliased to introduce appropriate gray-scale levels.

7.2.1 COLORED MNIST

We modify the MNIST dataset in the exact same manner as in [Arjovsky et al. \(2019\)](#). Specifically, [Arjovsky et al. \(2019\)](#) creates the dataset in a way that it contains both the invariant and spurious features according to different causal graphs. Spurious features are introduced using colors. Digits less than 5 (excluding 5) are attributed with label 0 and the rest with label 1. The dataset is divided across three clients, out of which two serve as training and one as testing. The 60,000 images from MNIST train set are divided equally amongst the two training clients i.e. each consists of 30,000 samples. The testing set contains the 10,000 images from the MNIST test set. Preliminary noise is added to the label to reduce the invariant correlation. Specifically, the initial label (\tilde{y}) of each image is flipped with a probability δ_k to construct the final label y . The final label y of each image is further flipped with a probability p_k to construct its color code (z). In particular, the image is colored red, if $z = 1$ and green if $z = 0$. The flipping probability which defines the color coding of an image, p_k is 0.2 for client 1, 0.1 for client 2 and 0.9 for the test client. The probability δ_k is fixed to 0.25 for all clients k . The above choice is defined in a way that the mean degree of label-color (spurious) correlation ($1 - p_k, \forall k$) is more than the average degree of invariant correlation ($1 - \delta_k, \forall k$). A sample batch of images elucidating the above construction is shown in Figure 4.

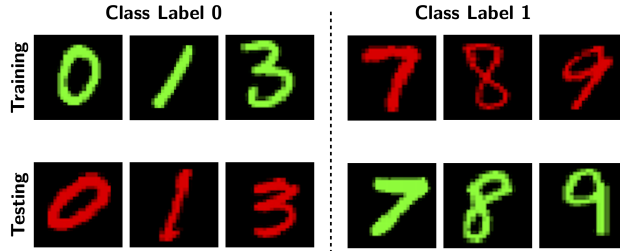


Figure 4: COLORED MNIST: Illustration of samples containing high spurious correlation between label and color during training. While testing, this correlation is significantly reduced as label 0 is highly correlated with the color mapped to label 1 and vice-versa.

7.2.2 COLORED FASHION MNIST

We use the exact same environment for creating COLORED FASHION MNIST as in [Ahuja et al. \(2020\)](#). The data generating process of COLORED FASHION MNIST is motivated from that of COLORED MNIST in a way that it possesses spurious correlations between the label and the colour. Fashion MNIST consists of images from a variety of sub-categories under the two broad umbrellas of clothing and footwear. Clothing items include categories like: “t-shirt”, “trouser”, “pullover”, “dress”, “shirt” and “coat” while the footwear category includes “sandal”, “sneaker”, “bag” and “ankle boots”. Similar to COLORED MNIST, the train dataset is equally split across two clients (30,000 images each) and the entire test set is attributed to the test client. Preliminary labels for binary classification are constructed such $\tilde{y} = 0$ for “t-shirt”, “trouser”, “pullover”, “dress”, “coat”, “shirt” and $\tilde{y} = 1$: “sandle”, “sneaker” and “ankle boots”. Next, we add noise to the preliminary label by flipping \tilde{y} with a probability $\delta_k = 0.25, \forall k$ to construct the final label y . We next flip the final label with a probability p_k to designate a color (z), with $p_1 = 0.2$ for the first client, $p_2 = 0.1$ for the

second client and $p_3 = 0.9$ for the test client. The image is colored red, if $z = 1$ and green if $z = 0$. A sample batch of images elucidating the above construction is shown in Figure 5.

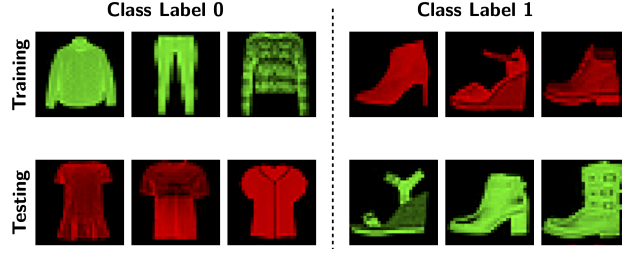


Figure 5: COLORED MNIST: Illustration of samples containing high spurious correlation between label and color during training. While testing, this correlation is significantly reduced as label 0 is highly correlated with the color mapped to label 1 and vice-versa.

7.2.3 SPURIOUS CIFAR10

In this setup, we modify the CIFAR-10 dataset similar to the COLORED MNIST dataset. Instead of coloring the images, we use a different mechanism based on the spatial location of a synthetic feature to generate spurious features. CIFAR10 dataset consists of 60,000 images from 10 classes including “airplane”, “automobile”, “bird”, “cat”, “deer”, “dog”, “frog”, “house”, “ship”, “truck”. The original dataset is relabelled to create a binary classification task between motor and non-motor objects. All images corresponding to the label “frog” are discarded to ensure a similar samples count for the two classes. Similar to COLORED MNIST, the train dataset is equally split across two clients and the entire test set is attributed to the test client. Preliminary labels for binary classification are constructed such $\tilde{y} = 0$ for “airplane”, “automobile”, “ship”, “truck” and $\tilde{y} = 1$: “bird”, “cat”, “deer”, “dog” and “horse”. Next, we add noise to the preliminary label by flipping \tilde{y} with a probability $\delta_k = 0.25, \forall k$ to construct the final label y . We next flip the final label with a probability p_k to designate a positional index (z), with $p_1 = 0.2$ for the first client, $p_2 = 0.1$ for the second client and $p_3 = 0.9$ for the test client. This index defines the spatial location of a 5×5 black patch in the image. An index value of 0 ($z = 0$) specifies the patch at the top left corner of the image, while an index value of 1 ($z = 1$) corresponds to a black patch over the top-right corner of the image. Based on the choice of flipping probabilities, images in the training set are spuriously correlated to the position of the patch in the image. Such correlation does not exist while testing. A sample batch of images elucidating the above construction is shown in Figure 6.

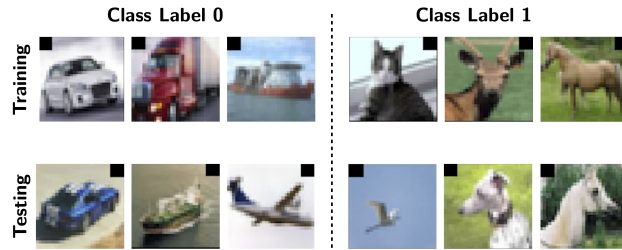


Figure 6: SPURIOUS CIFAR10: Illustration of samples containing high spurious correlation between labels and spatial location of the 5×5 black patch during training. While testing, this correlation is significantly reduced as label 0 is now highly correlated with the spatial location corresponding to label 1 and vice-versa.

7.2.4 Extended Datasets

We extend all the three datasets COLORED MNIST, COLORED FASHION MNIST and SPURIOUS CIFAR10 as in Choe et al. (2020) to robustly test our approach across multiple clients. Analogous to COLORED MNIST with two training environments ($N = 2$), we extend the datasets to incorporate $N = 2, 3, 5$ and 10 training clients. In particular, we attribute each client with a unique flipping probability p_k . For each value of N , the maximum value of $p_k, \forall k$ is 0.3, while the minimum value is 0.1. The values of p_k for each client are spaced evenly between this range. For example, for the case of $N = 5$ clients, the flipping probabilities of clients are $p_1 = 0.3, p_2 = 0.2$, and $p_3 = 0.1$. The flipping probability δ_k which decides the final label y is fixed to 0.25 for all clients. The maximum and the minimum values of p_k are chosen in a way that the average spurious correlation which is 0.8 is more than the invariant correlation i.e. 0.75.

Further, since all the previous settings were binary classification tasks, we extend the standard datasets COLORED MNIST, COLORED FASHION MNIST and SPURIOUS CIFAR10 over multi class classification Choe et al. (2020). Specifically, we extend the number of classes from 2 to 5 and 10. For COLORED FASHION MNIST and COLORED MNIST, a unique color is assigned to each output class such that the label is highly correlated ($\sim 80\% - 90\%$) with the color in the training set. In the test set, these correlations are significantly reduced (10%) by allowing high spurious correlations with the color of the following class. For instance, in testing, the color corresponding to class label 8 would be the one which was heavily correlated with class label 9 while training. This reduces the original spurious correlations and is hence useful for evaluating the extent to which the trained model has learned the invariant features. A sample batch of images elucidating the above construction is shown in Figure 7. We do not construct a multi-class classification setup for SPURIOUS CIFAR10 as it is difficult to find a unique spatial location in the image corresponding to each class (e.g. in case of 10-class classification).

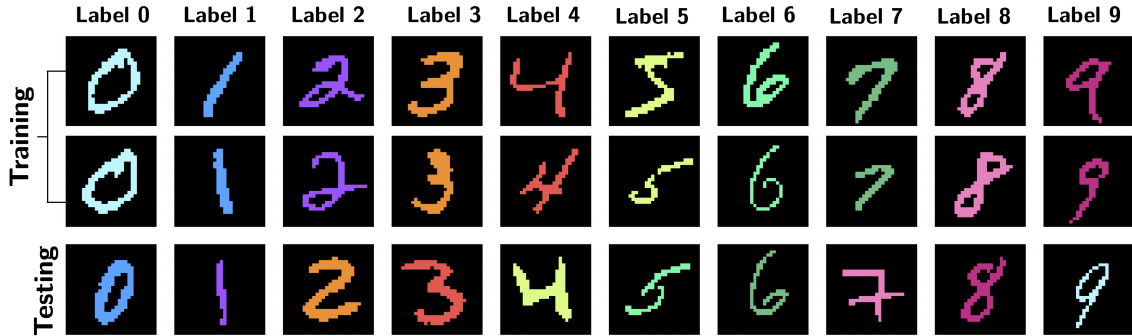


Figure 7: EXTENDED COLORED MNIST: Illustration of samples corresponding to a 10-digit classification task. During training, each class label is spuriously correlated with a unique color. While testing, this correlation is significantly reduced as each image is colored with the color corresponding to its succeeding label.

7.3 Experimental Setup

7.3.1 Architecture Details

For all the approaches using a fixed representation i.e. F-IRM GAMES, F-FL GAMES (SMOOTH), *parallelized* F-IRM GAMES and *parallelized* F-FL GAMES (SMOOTH), we use the architecture mentioned below. The architecture used to train a predictor at each client is a multi-layered perceptron with three fully connected (FC) layers. The details of layers are as follows:

- Flatten: A flatten layer that converts the input of shape (Batch Size, Length, Width, Depth) into a tensor of shape (Batch Size, Length * Width * Depth)
- FC1: A fully connected layer with an output dimension of 390, followed by ELU non-linear activation function
- FC2: A fully connected layer with an output dimension of 390, followed by ELU non-linear activation function
- FC3: A fully connected layer with an output dimension of 2 (Classification Layer)

This same architecture is used across approaches with fixed representation.

For the approaches with trainable representation i.e. V-IRM GAMES, V-FL GAMES (SMOOTH), *parallelized* V-IRM GAMES and *parallelized* V-FL GAMES (SMOOTH), we use the following architecture for the representation learner

- Flatten: A flatten layer that converts the input of shape (Batch Size, Length, Width, Depth) into a tensor of shape (Batch Size, Length * Width * Depth)
- FC1: A fully connected layer with an output dimension of 390, followed by ELU non-linear activation function

The output from FC1 is fed into the following architecture, which is used as the base network to train the predictor at each client:

- FC1: A fully connected layer with an output dimension of 390, followed by ELU non-linear activation function
- FC2: A fully connected layer with an output dimension of 390, followed by ELU non-linear activation function
- FC3: A fully connected layer with an output dimension of 2 (Classification Layer)

This architecture is used across approaches with variable representation.

7.3.2 Optimizer and other hyperparameters

We use a different set of hyper-parameters based on the dataset. In particular,

- COLORED MNIST and COLORED FASHION MNIST: For fixed representation, we use Adams optimizer with a learning rate of $2.5e-4$ across all experiments (sequential or parallel). For the variable representation, we use Adams optimizer with a learning rate of $2.5e-5$ for the representation learner and the same optimizer with a learning rate of $2.5e-4$ for the predictor at each client.
- SPURIOUS CIFAR10: For fixed representation, we use Adams optimizer with a learning rate of $1.0e-4$ across all experiments (sequential or parallel). For the variable representation, we use Adams optimizer with a learning rate of $9.0e-4$ for the representation learner and the same optimizer with a learning rate of $1.0e-4$ for the predictor at each client.

For all the experiments, we fix the batch size to 256 and optimize the Cross Entropy Loss. We use the same termination criterion as in [Ahuja et al. \(2020\)](#). Specifically, we stop training when the observed oscillations become stable and the ensemble model is in a lower training accuracy state. We choose a training threshold and terminate the training as soon as the training accuracy drops below this value. In order to ensure stability of oscillations,

we set a period of warm start. In this period, the training is not stopped even if the accuracy drops below the threshold. For variable representation, the duration of this warm start period is set to the number of training steps in an epoch i.e. (training data size/ batch size). However, for the approaches with fixed representation, this period is fixed to N rounds where N is the number of training clients. In particular, for two clients, the warm start period ends as soon as the second client finishes playing its optimal strategy for the first time.

7.4 Additional Results and Analysis

7.4.1 Robustness to the number of Outcomes

As described in Section 7.2.4, we test the robustness of our approach to an increase in number of output classes. We compare F-IRM GAMES and *parallelized* F-IRM GAMES across 2-digit, 5-digit and 10-digit classification for COLORED MNIST and COLORED FASHION MNIST.

As shown in Tables 4 and 5, both the sequential and the parallel version of IRM GAMES i.e. F-IRM GAMES and *parallelized* F-IRM GAMES respectively are robust to an increase in the number of output classes. For both the datasets, *parallelized* F-IRM GAMES performs at par or better than F-IRM GAMES.

Table 4: COLORED MNIST: Comparison of F-IRM GAMES and F-IRM GAMES (Parallel) with increasing number of output classes, in terms of the training and testing accuracy (mean \pm std deviation). Here ‘Seq.’ is an abbreviation used for ‘Sequential’, which denotes F-IRM GAMES.

Type	# Classes	TRAIN ACCURACY	TEST ACCURACY
Seq.	2	75.13 \pm 1.38	68.40 \pm 1.83
	5	79.39 \pm 0.91	69.90 \pm 3.16
	10	82.27 \pm 0.76	69.22 \pm 3.11
Parallel	2	71.71 \pm 8.23	69.73 \pm 2.12
	5	78.61 \pm 2.86	68.42 \pm 2.54
	10	82.17 \pm 1.21	69.29 \pm 3.17

Table 5: COLORED FASHION MNIST: Comparison of F-IRM GAMES and F-IRM GAMES (Parallel) with increasing number of output classes, in terms of the training and testing accuracy (mean \pm std deviation). Here ‘Seq.’ is an abbreviation used for ‘Sequential’, which denotes F-IRM GAMES.

Type	# Classes	TRAIN ACCURACY	TEST ACCURACY
Seq.	2	50.36 \pm 2.78	47.36 \pm 4.33
	5	77.28 \pm 1.54	69.35 \pm 0.66
	10	80.02 \pm 0.38	71.22 \pm 3.00
Parallel	2	55.06 \pm 2.04	52.07 \pm 1.60
	5	77.61 \pm 1.51	70.83 \pm 0.96
	10	80.12 \pm 0.78	70.39 \pm 2.28

7.5 Effect of Simultaneous BRD

Similar to the experiments conducted for COLORED MNIST, where we compared F-IRM GAMES and *parallelized* F-IRM GAMES across an increase in the number of clients, we replicate the same setup for COLORED FASHION MNIST and SPURIOUS CIFAR10. We

report the results on both datasets in Figures 8 and 9. Consistent with the results on COLORED MNIST, as the number of clients in the FL system increases, there is a sharp increase in the number of communication rounds required to reach equilibrium. However, the same doesn't hold true for *parallelized* F-IRM GAMES. Further, the accuracy achieved by *parallelized* F-IRM GAMES is comparable or better than that achieved by F-IRM GAMES.

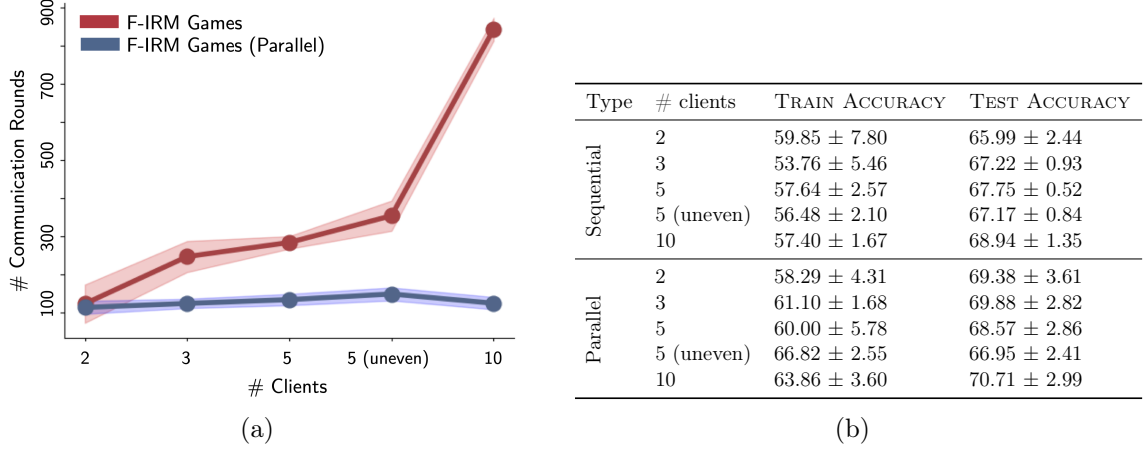


Figure 8: COLORED FASHION MNIST: (a) Number of communication rounds required to achieve the Nash equilibrium versus the number of clients in the FL setup; (b) Comparison of F-IRM GAMES and F-IRM GAMES (Parallel) with an increase in the number of clients, in terms of training and testing accuracy (mean \pm std deviation).

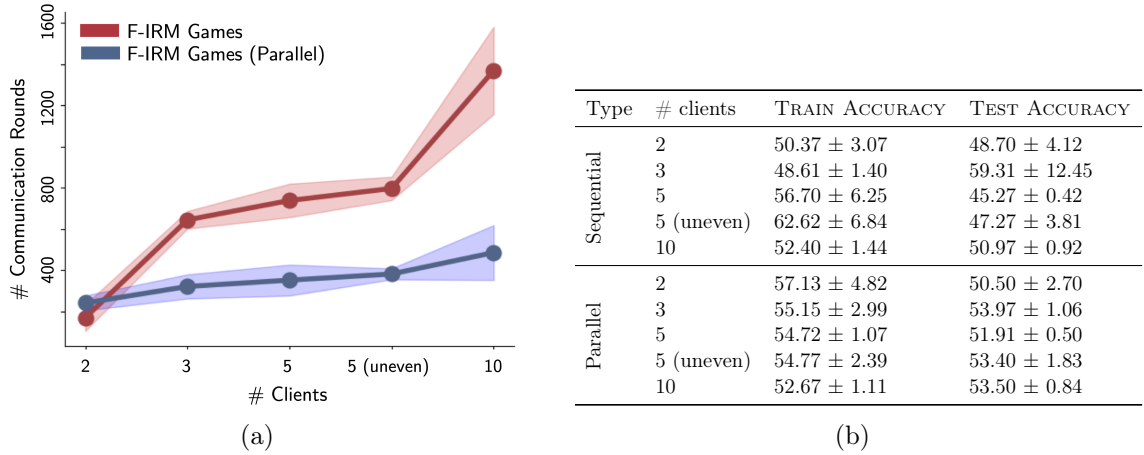


Figure 9: SPURIOUS CIFAR10: (a) Number of communication rounds required to achieve the Nash equilibrium versus the number of clients in the FL setup; (b) Comparison of F-IRM GAMES and F-IRM GAMES (Parallel) with an increase in the number of clients, in terms of training and testing accuracy (mean \pm std deviation).

7.5.1 Effect of Memory Ensemble

Similar to the experiments conducted for COLORED MNIST, where we compared F-IRM GAMES and F-FL GAMES (SMOOTH), we replicate the same setup for COLORED FASHION MNIST and SPURIOUS CIFAR10. We report the results on both datasets in Figures 10 and 11.

Consistent with the results on COLORED MNIST, performance curves oscillate at each step for F-IRM GAMES while the oscillations in F-FL GAMES (SMOOTH) are observed after

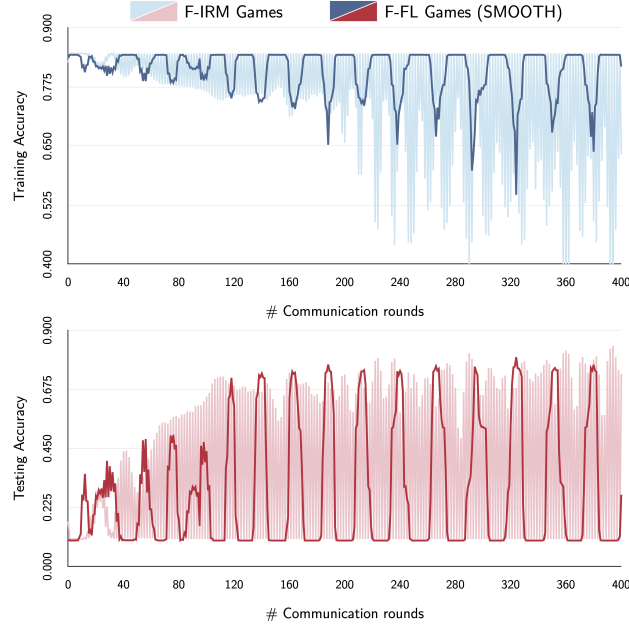


Figure 10: COLORED FASHION MNIST: Evolution of Training and Testing Training for F-IRM GAMES and F-FL GAMES (SMOOTH) using a buffer size of 5, over the number of communication rounds

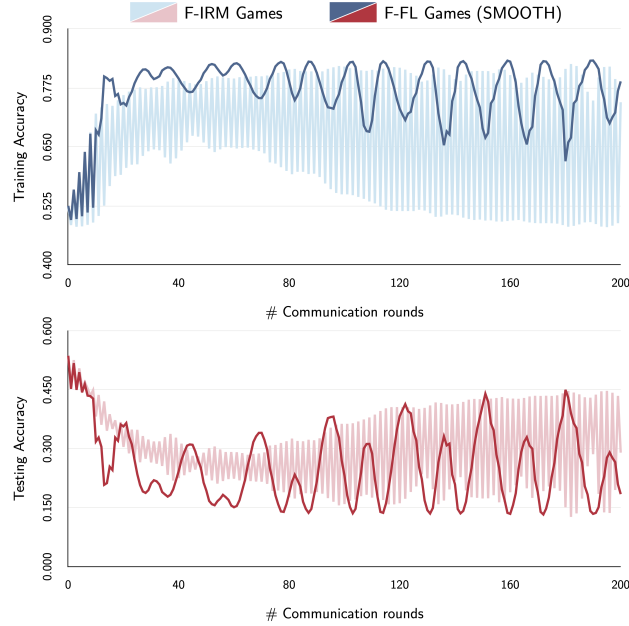


Figure 11: SPURIOUS CIFAR10: Evolution of Training and Testing Training for F-IRM GAMES and F-FL GAMES (SMOOTH) using a buffer size of 5, over the number of communication rounds

an interval of roughly 40 rounds for both the datasets. Further, F-FL GAMES (SMOOTH) also achieves high testing accuracy. This implies that it does not rely on the spurious features to make predictions. Similar performance evolution curves are also observed for *parallelized* F-FL GAMES (SMOOTH) with an added benefit of faster convergence as compared to F-IRM GAMES and F-FL GAMES (SMOOTH).

7.5.2 Effect of using Gradient Descent (GD) for ϕ

Similar to the experiments conducted for COLORED MNIST, where we compared V-IRM GAMES and V-FL GAMES (SMOOTH+FAST), we replicate the same setup for COLORED FASHION MNIST and SPURIOUS CIFAR10. We report the results on both datasets in Figures 12 and 13. Consistent with the results on COLORED MNIST, V-FL GAMES (SMOOTH+FAST) is able to achieve significantly higher testing accuracy in fewer communication rounds as compared to V-IRM GAMES on both the datasets.

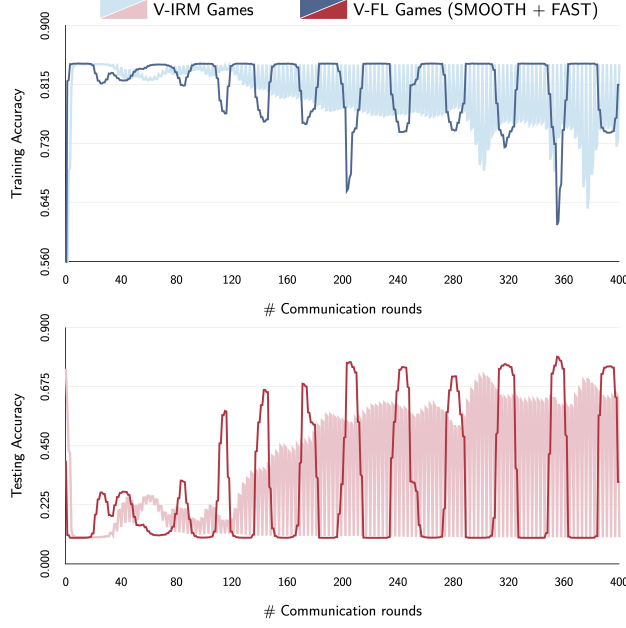


Figure 12: COLORED FASHION MNIST: Evolution of Training and Testing Training for V-IRM GAMES and V-FL GAMES (SMOOTH + FAST) using a buffer size of 5, over the number of communication rounds

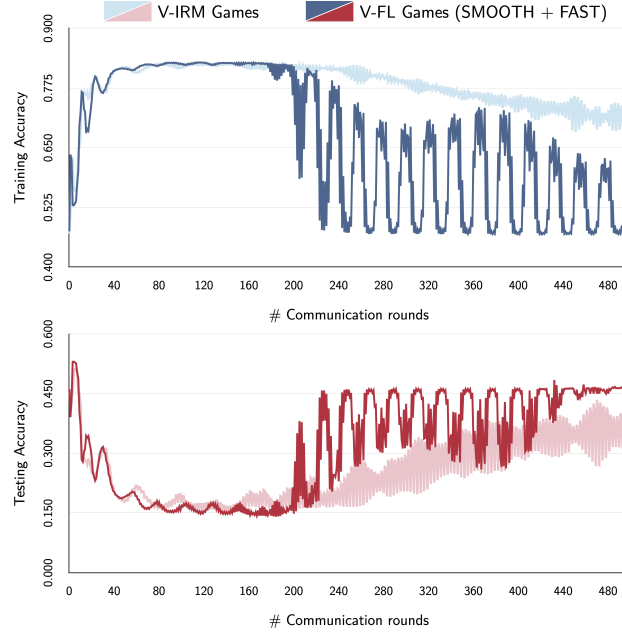


Figure 13: SPURIOUS CIFAR10: Evolution of Training and Testing Training for V-IRM GAMES and V-FL GAMES (SMOOTH+FAST) using a buffer size of 5, over the number of communication rounds

7.5.3 Effect of exact best response

Similar to the experiments conducted for COLORED MNIST, where we studied the influence of increasing the amount of local computation at each client, we replicate the setup for COLORED FASHION MNIST and SPURIOUS CIFAR10.

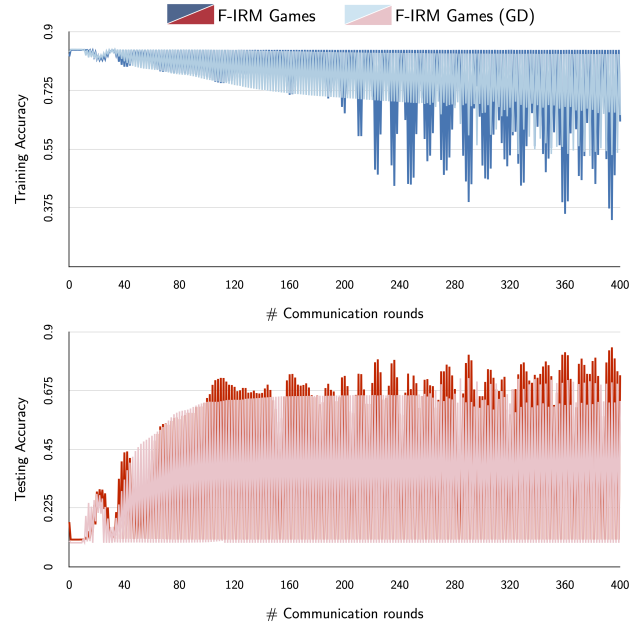


Figure 14: COLORED FASHION MNIST: Evolution of Training and Testing Training when doing a gradient descent to update the predictor at each client versus the standard training paradigm i.e. F-IRM GAMES, over the number of communication rounds.

Consistent with the results on COLORED MNIST and as shown in Figures 14 and 15, even when the number of local steps at each client reaches its maximum i.e. (training data

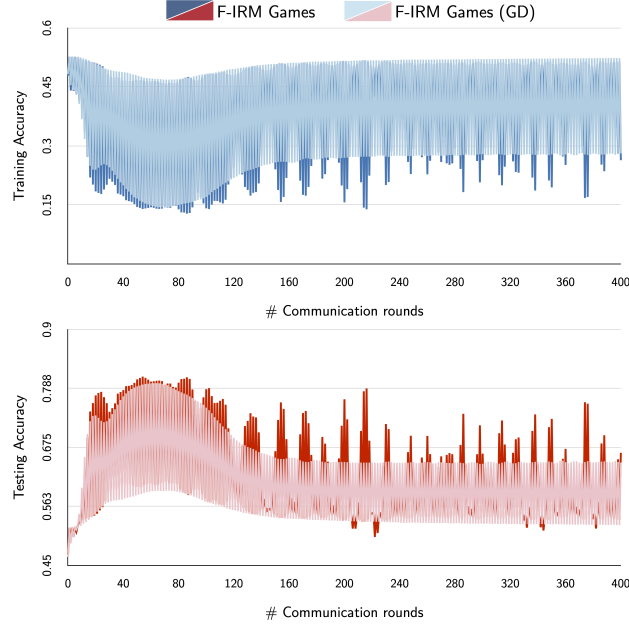


Figure 15: SPURIOUS CIFAR10: Evolution of Training and Testing Training when doing a gradient descent to update the predictor at each client versus the standard training paradigm i.e. F-IRM GAMES, over the number of communication rounds.

size/ mini-batch size)), the trained models are able to achieve high testing accuracy at equilibrium. Further, we can also conclude from Figures 14 and 15 that this setup achieves faster convergence with a slight change in the training accuracy at equilibrium. As observed from the empirical results and discussed by Ahuja et al. (2021b), IRM GAMES exhibits convergence guarantees despite an increase in the amount of local compute. This has direct implications towards training stability and building communication efficient FL systems.